microRNA-21 upregulates YAP by inhibiting transcription factor RUNX1 to regulate immunosuppressive ability of myeloid-derived suppressor cells in lung cancer

Guangping Meng
the Second Hospital of JilinUniversity
Jinying Wei
the Second Hospital of Jilin University
Yanjun Wang
the Second Hospital of Jilin University
Danhua Qu
the Second Hospital of Jilin University
Jie Zhang (zjie2019@163.com)
the Second Hospital of Jilin University

Research

Keywords: Lung cancer, microRNA-21, Runt-related transcription factor 1, Yes-associated Protein, Myeloid-derived suppressor cells, Immunosuppressive ability

Posted Date: April 8th, 2020

DOI: https://doi.org/10.21203/rs.3.rs-21173/v1

Abstract

Background Lung cancer is one of the most frequently fatal cancers. The microRNA-21 (miR-21) has a known oncogenic function on immune cells in tumors, but its biological role and clinical significance in immunosuppression of lung cancer remains largely enigmatic. Our study aims to explore the role and molecular mechanisms of miR-21 in lung cancer.

Methods We observed that miR-21 and YAP were highly expressed, while RUNX1 was poorly expressed in lung cancer tissues and cell lines. The loss- and gain- function approaches were performed to determine the roles of miR-21, RUNX1 or YAP in the immunosuppressive ability of myeloid-derived suppressor cells (MDSCs) in lung cancer.

Results MiR-21 inhibition, YAP knockdown or RUNX1 overexpression reduced the proportion of MDSCs in lung cancer tissue and peripheral blood, but increased the proportion of T helper (Th) and CTL. Furthermore, miR-21 inhibition, YAP knockdown or RUNX1 overexpression increased apoptosis of MDSCs, more cells at G0/G1 phase, fewer cells at G2/M phase, but reduced IL-10, TGF-β and GM-CSF levels. The effect of miR-21 and RUNX1 on tumor growth was verified by xenograft tumors in nude mice.

Conclusions Taken together, miR-21 upregulates YAP expression by inhibiting RUNX1 and consequently promotes the immunosuppressive ability of MDSCs against lung cancer.

Background

Lung cancer is one of the frequently diagnosed cancers around the world and remains a chief cause of cancer-associated mortality in both men and women [1]. Less than 7% of patients survive 10 years after diagnosis across all lung cancer stages [2]. Metastasis to other organs, especially the brain, is responsible for the high mortality rate of lung cancer [3]. The therapeutic potential of combining epigenetics targeted drugs and chemotherapy, targeted therapy or immunotherapy has been recently investigated [4]. Moreover, positioning and repositioning of chromosome may be involved in the sensitivity of lung cancer cells and lung carcinogenesis mechanism [5]. However, the molecular mechanisms governing this event are not fully elucidated.

MicroRNAs (miRNAs), endogenous RNAs of about 21 nucleotides in length, play regulatory roles in animals and plants [6]. The capability of miRNAs to regulate the expression of oncogenic pathways and their vital roles in lung cancer progression indicate miRNAs as novel prognostic biomarkers or targets for treatment [7]. Overexpression of miR-21-5p by mesenchymal stem cell-secreted extracellular vesicles (MSC-EVs) promotes lung cancer development [8]. Moreover, suppressing miR-21 inhibits cell migration and invasion in non-small cell lung carcinoma (NSCLC) cells [9]. In the current study, microarray-based analysis predicted RUNX1 to be one of the downstream target genes by miR-21. The runt-related transcription factor (RUNX) family (RUNX1, RUNX2, and RUNX3), which is involved in many cell lineages, has been associated with the development of cancer [10, 11]. RUNX1, a core-binding factor in transcription families, is one of the most commonly mutated genes found in many hematological

malignancies [12]. A prior study has shown that RUNX1 can inhibit Yes-associated protein (YAP) to accelerate the occurrence of tumor [13]. Therapeutic activation of YAP, a Hippo pathway effector, causes severe side effects in human cancer developments [14, 15]. MiR-129 is found to directly suppress the expression of RUNX1 and evoke the transcriptional modulation by RUNX1 [16]. In this regard, we hypothesized that a regulatory network of the miR-21/RUNX1/YAP axis may be involved in the treatment in lung cancer. Therefore, the current study was conducted with the aim to verify the expected involvement of the miR-21/RUNX1/YAP axis in lung cancer, and to elucidate the underlying molecular mechanisms.

Materials And Methods

Ethics statement

All animal experiments and procedures were approved by the Institutional Animal Care and Use Committee of the Second Hospital of Jilin University. The animal experiments were conducted based on minimized animal numbers and discomfort of experimental animals.

Microarray-based analysis

The lung cancer related miRNA dataset GSE63805 was downloaded from the Gene Expression Omnibus (GEO) database (https://www.ncbi.nlm.nih.gov/gds). There were 62 tissue samples in GSE63805, including 30 normal lung samples and 32 lung cancer samples. Differential analysis of the expression datasets was performed by the limma package (http://www.bioconductor.org/packages/release/bioc/html/limma.html) in R language, with the threshold (|logFC|>1, $p < 0.01$). The miRNA with the lowest p value was selected for following analysis. The downstream target genes of the miRNA were predicted by mirDIP (Integrated Score > 0.2) (http://ophid.utoronto.ca/mirDIP/) and starbase (clipExpNum ≥ 3) (http://starbase.sysu.edu.cn), and differential expression analysis of the lung cancer dataset GSE74706 also was performed in R language (|logFC|>1, $p < 0.01$). There were 36 samples in the GSE74706 dataset, including 18 normal and 18 lung cancer samples. Then, the human transcription factors were obtained from the Cistrome database (http://cistrome.org), and these results were intersected to determine the downstream target gene of miR-21 based on the existing studies. Next, the related genes of the target gene were identified according to the GeneMANIA database (http://genemania.org), and Cistrome was used to obtain genes with a correlation greater than 0.35 or less than − 0.35 with the expression of downstream genes of target transcription factors in lung adenocarcinoma. The intersection of GeneMANIA and Cistrome results was adopted to obtain the downstream genes of key target transcription factors. The comprehensive data of lung adenocarcinoma and squamous cell carcinoma in the Cancer Genome Atlas (TCGA) database (http://gepia.cancer-pku.cn) were analyzed by the Gene Expression Profiling Interactive Analysis (GEPIA) database (http://gepia.cancer-pku.cn) to confirm the correlation of expressions between the target transcription factors and their downstream genes, and starBase was used to determine the binding site of miRNA and target transcription factors.

Cell culture and treatment

Lewis lung cancer cells were purchased from Cancer Research Institute of Chinese Academy of Medical Sciences (Beijing, China). Cells were cultured in Dulbecco's Modified Eagle Medium (DMEM) containing 10% fetal bovine serum, 100 U/mL penicillin and 100 U/mL streptomycin at 37°C in a humidified atmosphere with 5% CO_2. The cells were observed daily as they grew into a monolayer adhering to the chamber walls. When the cells were in a logarithmic growth phase, they were trypsinized and passaged with 0.25% trypsin solution once every 2–3 days. The ratio of living cells was assessed by trypan blue staining. The cell concentration was diluted to 1×10^7 cells/mL in phosphate buffer saline (PBS), and the cell suspension was prepared for the following experiments.

Animal model establishment

A total of 72 C57BL/6 mice with half males and half females (aged 5–6 weeks, purchased from Beijing Vital River Laboratory Animal Technology Co., Ltd., Beijing, China) were selected. The mice of the average weight of (20 ± 0.5) g were numbered after acclimation for 1 week, and 8 of them (half male and half female) were randomly selected as the blank control, and subcutaneously injected with 0.4 mL normal saline into the armpit of the right forelimb. Then the remaining 64 mice were inoculated with 0.2 mL Lewis lung cancer cell suspension (about 2×10^6 tumor cells). The tumor growth was observed and measured three days later.

When the tumor diameter had reached about 5 mm (around the 5th day), every 8 mice (half male and half female) were infected with lentiviral particles containing miR-21 antagomir negative control (NC), miR-21 antagomir, miR-21 antagomir NC combined with sh-NC, miR-21 antagomir combined with sh-NC, miR-21 antagomir combined with sh-RUNX1, miR-21 antagomir NC combined with oe-NC, miR-21 antagomir combined with oe-NC, or miR-21 antagomir combined with oe-YAP, respectively. In brief, mice were intraperitoneally injected with 4 mg/kg normal saline (antagomir NC) or the same amount of miR-21 antagomir, and other mice were also intraperitoneally injected with the same amount of lentiviral particles or normal saline for 5 times, respectively. Then, on the 7th, 14th and 21st day after injection, the blood sample was collected from each mouse, and the tumor diameter was measured and recorded.

Preparation of mouse tumor and peripheral blood cell suspension

After about 3 weeks of subcutaneous injection of Lewis lung cancer cells, mice were anesthetized with intraperitoneal injection of 3% pentobarbital sodium at a dose of 50 mg/kg. Peripheral blood samples taken from orbit were put in 15 mL centrifuge tube (containing 1 mL anticoagulant). The mice were euthanized with cervical dislocation and displaced in 75% alcohol for 5 minutes. Then, the mice were fixed on a foam board, and the tumors were removed by scissors and forceps, before the tumors were placed into the 24-well plate with l mL PBS.

The tumor suspension was prepared as follows. In brief, the resected tumor was photograph and its length and width were measured with a vernier caliper, and the tumor volume was calculated as (length × width × width)/2. The tumor was cut with scissors into small portions in a 24 hole plate, transferred into a 15 mL centrifuge tube, added with 2 mL 1640 culture solution and 60 μL collagenase, and incubated in a shaker at 37℃ for 3 hours. After that, the centrifuge tube was mixed by vortexing, and added with PBS to a constant volume of 10 mL. After centrifugation, the supernatant was discarded and 2 mL PBS was added into the tube. Next, the solution was passed through a sieve into a 15 mL centrifuge tube, re-centrifuged and the supernatant was discarded. Finally, PBS was added to make the tumor cell suspension.

The peripheral blood cell suspension was prepared. In brief, 1 mL PBS was added into the 15 mL centrifuge tube containing anticoagulant, centrifuged and the supernatant was discarded. Upon addition of 3 mL of hemolytic solution, the tube was put aside for 4–5 minutes, and added with PBS to obtain the peripheral blood cell suspension.

Flow cytometry for cell characterization

MDSCs were characterized as follows. A total of 50 μL of peripheral blood or tumor local cell suspension was transferred respectively into 2 mL centrifuge tubes, and 0.5 μL of CD45.2, CD11b and Gr-1 (BD Biosciences, Franklin Lakes, NJ, USA) was added to each tube. Then the tubes were then added with 48 μL of PBS, and stained in a refrigerator at 4℃ for 20 minutes. Then, the tubes were added with 1 mL of PBS and centrifuged at 300 rpm for 5 minutes, added with 100 μL PBS for resuspension, and finally analyzed with a flow cytometer.

T cell phenotype was detected. Briefly, 50 μL of peripheral blood and tumor local cell suspension was placed into 2 mL centrifuge tubes, and then mixed with 0.5 μL of CD45.2, CD4 and CD8a (BD Biosciences, Franklin Lakes, NJ, USA). Then, 48 μL of PBS was added to the tubes for staining in the refrigerator at 4℃ for 20 minutes. Then, the tubes were added with another 1 mL of PBS and centrifuged at 300 rpm. After removing the supernatant, 100 μL PBS was added for resuspension and analysis with a flow cytometer.

Flow cytometry for cell proliferation

Lymphocyte isolating medium was adopted to separate cells in tumor tissues and peripheral blood samples. Then, the $CD4^+$ or $CD8^+$ T cells in the samples were separated using a $CD4^+$ or $CD8^+$ T cell separation kit (Miltenyi Biotec, Bergisch Gladbach, Germany). According to the manufacturer's instructions (Invitrogen Inc., Carlsbad, CA, USA), $CD4^+$ or $CD8^+$ T cells were labeled with 5-(and 6)-carboxyfluorescein diacetate, succinimidylester (CFSE), and stimulated with Con A (Sigma-Aldrich Chemical Company, St Louis MO, USA). MDSCs and T cells were derived from mice infected with lentiviral particles or control mice in the co-culture experiments. For a single co-culture, the T cells and the MDSCs were derived from the same mice. Then, the T cells were co-cultured with MDSCs at the proportions of 2:1, 4:1, 10:1 or 100:1 in 96 well plates for 96 hours. On the fourth day, the cells were analyzed by a flow

cytometer. The proliferation data from MDSCs were obtained through the gradient experiments on average.

MDSC sorting of peripheral blood

The mice were euthanized, and the peripheral blood was collected, followed by removal of red blood cells with red blood cell lysis buffer. Then, the lysed blood was incubated at 4℃ for 15 minutes with the addition of biotion-conjugated anti-Gr-1 (BD Biosciences, Franklin Lakes, NJ, USA), and then added with anti-biotion beads and incubated in the dark at 4℃ for 15 minutes. After washing, the blood was resuspended with PBS and MDSC sorting was performed using a LS column from Miltenyi Biotec (Bergisch Gladbach, Germany), following the manufacturer's instructions.

Flow cytometry for cell cycle analysis

MDSCs were collected and the cell concentration was adjusted to 1×10^6 cells/mL. Then, the cells were seeded into 24 well plates, and treated with antagomir NC + sh-NC, miR-21 antagomir + sh-NC, miR-21 antagomir + sh-RUNX1, antagomir NC + oe-NC, miR-21 antagomir + oe-NC, or miR-21 antagomir + oe-YAP. After 24 hours, the cells were collected, centrifuged at 2000 rpm for 5 minutes, fixed with 70% ethanol precooled at 4℃, and stored at 4℃. Before staining, the fixed solution was washed off with PBS, and cells were resuspended with the addition of 200 μL PBS. A total of 100 μL RNase A was added into the cells in water bath at 37℃ for 30 minutes, whereupon 400 μL propidium iodide (PI) was added. The mixture was then dyed at 4℃for 30 minutes in the dark. Before analysis, the cells were screened through a 200-mesh cell sieve, and added with 300 μL PBS to adjust the cell density. Then the cell cycle was analyzed by a flow cytometer, with the red fluorescence recorded at 488 nm, and 10000 cells were counted.

Annexin V-FITC/PI analysis

MDSCs were collected and the cell density was adjusted to 1×10^6 cells/mL. Then, the cells were seeded into 24 well plates, and infected with antagomir NC + sh-NC, miR-21 antagomir + sh-NC, miR-21 antagomir + sh-RUNX1, antagomir NC + oe-NC, miR-21 antagomir + oe-NC, or miR-21 antagomir + oe-YAP. After 24 hours, the cells were centrifuged at 2000 rpm for 5 minutes, washed twice with PBS, and suspended with the addition of 100 μL of binding buffer. The Annexin V-FITC kit was used for staining. A total of 5 μL Annexin V-FITC was added to the cell suspension, and then 5 μL PI was added and reacted for 15 minutes in the dark. Next, the cells were passed through a 200 mesh cell sieve. Finally, the cells were analyzed by a flow cytometer with the excitation wavelength at 488 nm and the emission wavelength at 530 nm, and 10000 cells were counted.

Enzyme linked immunosorbent assay (ELISA)

The eyeballs of mice were removed to collect blood samples, which were stored overnight at 4℃, and then centrifuged at 3500 × g. The clear serum from the upper layer was stored at -80℃. The serum levels of interleukin 10 (IL-10), transforming growth factor-beta (TGF-β) and granulocyte-macrophage colony stimulating factor (GM-CSF) were measured by ELISA kit. The serum was cultured for 24 hours,

whereupon the culture medium was collected, centrifuged at room temperature for 10 minutes at 1000 × g, and the supernatant was taken. The standard curve was drawn and the contents of IL-10, TGF-β and GM-CSF in the cell culture medium were measured in strict accordance with the instructions of the kit. The above kits were all purchased from Wuhan Xinqidi Biological Technology Co. Ltd. (Wuhan, China).

RNA immunoprecipitation (RIP) assay

Lewis lung cancer cells were lysed with radio-immunoprecipitation assay (RIPA) cell lysis buffer (P0013B, Beyotime Biotechnology Co., Shanghai, China) on ice bath for 5 minutes, and centrifuged at 12000 × g and 4℃ for 10 minutes. One portion of the cell extract was removed to serve as input, and the other part was incubated with antibody for co-precipitation. Each co-precipitation reaction system was washed with 50 μL magnetic beads and resuspended in 100 μL RIP wash buffer, and then incubated with 5 μg antibody for binding. After washing, the magnetic beads-antibody complex was resuspended in 900 μL RIP wash buffer and incubated overnight with 100 μL cell supernatant at 4℃. Samples were then placed on magnetic pedestals to collect beads-protein complexes, whereupon the samples and input were detached by treatment with protease K to extract RNA for subsequent polymerase chain reaction (PCR) analysis. The antibodies used here were anti-RUNX1 (ab92336, Abcam Inc., Cambridge, UK) and immunoglobulin G (IgG, ab150077, Abcam Inc., Cambridge, UK), which served as NC.

Chromatin immunoprecipitation (ChIP) assay

The Lewis lung cancer cells were fixed with formaldehyde for 10 minutes to induce DNA-protein cross-linking. The, an ultrasonicator was used to break the chromatin into fragments for 15 cycles of ten seconds each, with intervals of ten seconds. After that, the supernatant was collected, divided into two equal portions, and centrifuged at 12,000 × g for 10 minutes at 4℃. The IgG (ab150077, Abcam Inc., Cambridge, UK) and protein specific antibody anti-RUNX1 (ab92336, Abcam Inc., Cambridge, UK) were added into the two tubes, respectively, which were incubated at 4℃ overnight. The DNA-protein complex was precipitated by Protein Agarose/Sepharose, and centrifuged at 12,000 × g for 5 minutes. The supernatant was discarded and the nonspecific complex was washed to remove the cross-linking with incubation at 65℃ overnight. The DNA fragments were extracted and purified with phenol/chloroform, and the binding of RUNX1 and YAP promoter was measured by RT-qPCR with YAP promoter region specific primers.

Dual luciferase reporter gene assay

The wild type and mutant reporter plasmids of RUNX1-3’utr (pGL3-wt-RUNX1-3’utr, pGL3 -mut-RUNX1-3’utr) were designed and provided by Shanghai GenePharma Co. Ltd. (Shanghai, China). The Lewis lung cancer cells were co-transfected with antagomir NC and miR-21 antagomir with wt-RUNX1-3’utr and mut-RUNX1-3’utr respectively. After 48 hours, the cells were collected and lysed. The dual luciferase reporter gene assay system (Promega Corporation, Madison, WI, USA) was used for the detection of luciferase activity.

Immunohistochemistry

The paraffin-embedded tumor tissues slices were dewaxed with xylene I and II (Shanghai Sangon Biotechnology Co. Ltd., Shanghai, China) for 10 minutes, rehydrated with 100%, 95% and 70% gradient ethanol (Shanghai Sangon Biotechnology Co. Ltd., Shanghai, China) for 2 minutes each. Then, the tissues were immersed in 3% H_2O_2 for 10 minutes and antigen retrieval was performed by high pressure in a pressure cooker for 90 seconds. The tissues were cooled at room temperature and cut into slices, which were blocked with 5% bovine serum albumin (BSA), incubated at 37℃ for 30 minutes, added with 50 μL RUNX1 rabbit polyclonal antibody (ab92336, Abcam Inc., Cambridge, UK) and YAP rabbit monoclonal antibody (ab52771, Abcam Inc., Cambridge, UK) for incubation at 4℃ overnight. The next day, after washing with PBS for 2 minutes, the slices were added with 50 μL HRP labeled goat anti-rabbit antibody (ab6721, Abcam Inc., Cambridge, UK), incubated at 37℃ for 30 minutes and added with single antigen beads (SAB). Then, the slices were added with diaminobenzidine (DAB) solution (Fuzhou Maixin Biotechnology Development Co. Ltd. Fuzhou, China) for color development, re-stained with hematoxylin (Sigma-Aldrich, SF, CA, USA) for 5 minutes, and finally observed and photographed under an optical microscope (XSP-36, Bostar Optical Instruments Co., Ltd, Shenzhen, China). A total of 100 cells in each field were counted in 5 randomly selected high power visual fields, and the mean proportion of positive cells was calculated.

RT-qPCR

Total RNA was extracted using the RNeasy Mini Kit (Qiagen company, Hilden, Germany). The cDNA was synthesized using the reverse transcription kit (RR047A, Takara Bio Inc., Otsu, Shiga, Japan) and the miRNA first strand cDNA synthesis first (tailing reaction) kit (B532451-0020, Shanghai Sangon Biotechnology Co. Ltd., Shanghai, China). RNA loading was performed using the SYBR® Premix Ex Taq™ II (Perfect Real Time) kit (DRR081, Takara Bio Inc., Otsu, Shiga, Japan). RT-qPCR was carried out in a real-time PCR instrument (ABI 7500, ABI Company, Oyster Bay, NY). The general negative primer for miRNA and the upstream primer for glyceraldehyde-3-phosphate dehydrogenase (GAPDH) were provided by miRNA First Strand cDNA Synthesis (Tailing Reaction) kit, and other primers were synthesized by Shanghai Sangon Biotechnology Co. Ltd. (Shanghai, China) (Table 1). The Ct value of each well was recorded. GAPDH or U6 were taken as internal references, and the relative expression of each gene was calculated by the $2^{-\Delta\Delta Ct}$ method.

Table 1

The primer sequences of RT-qPCR

Gene	Primer sequences
miR-21 (hsa)	F: GGACTAGCTTATCAGACTG
	R: CATCAGATG CGTTGCGTA
miR-21 (mus)	F: GACATCGCATGGCTGTACCA
	R: CCATGAGATTCAACAGTCAACATC
RUNX1	F: TGATGGCTGGCAATGATGAA
	R: TGCGGTGGGTTTGTGAAGAC
YAP	F: CGCTCTTCAACGCCGTCA
	R: AGTACTGGCCTGTCGGGAGT
ARG-1	F: CTCCAAGCCAAAGTCCTTAGAG
	R: AGGAGCTGTCATTAGGGACATC
iNOS	F: CCAAGCCCTCACCTACTTCC
	R: CTCTGAGGGCTGACACAAGG
GAPDH	F: TGAAGCAGGCATCTGAGGG
	R: CGAAGGTGGAAGAGTGGGAG
U6	F: CTCGCTTCGGCAGCACA
	R: AACGCTTCACGAATTTGCGT

Notes: RT-qPCR, reverse transcription quantitative polymerase chain reaction; RUNX1, runt-related transcription factor 1; YAP, yes-associated protein; ARG-1, Arginase-1; iNOS, inducible nitricoxide synthase; GAPDH, glyceraldehyde-3-phosphate dehydrogenase; F, forward ,R, reverse.

Western blot analysis

The total protein in tissues or cells was extracted by radioimmunoprecipitation assay (RIPA) containing phenylmethylsulfonyl fluoride (PMSF). Bicinchoninic acid (BCA) kit was used to measure the total protein concentration. A total of 50 μg protein was dissolved in 2 × sodium dodecyl sulfate (SDS) sample buffer and boiled at 100℃ for 5 minutes. The protein was separated by a sodium dodecyl sulfate–polyacrylamide electrophoresis (SDS-PAGE) and transferred onto a polyvinylidene fluoride (PVDF) membrane, and sealed with 5% skim milk solution at room temperature for 1 hour. The membrane was incubated overnight at 4℃ with primary antibodies purchased from Abcam (Cambridge, UK): rabbit anti-RUNX1 (ab92336), rabbit anti-YAP (ab52771), rabbit anti-ARG-1 (ab133543), iNOS (ab3523), and GAPDH (ab181602) as internal reference. Then, the membrane was washed three times with tris-buffered saline

with Tween 20 (TBST) for 10 minutes each time. The membrane was then incubated with horseradish peroxidase (HRP) labeled goat anti-rabbit IgG H&L (ab6721, Abcam, Cambridge, UK) for 1 hour, developed with an enhanced chemiluminescence (ECL) fluorescence test kit (BB-3501, Amersham, Chicago, Illinois, USA), and exposed in a gel imager. The membrane was digitally photographed using the Bio-Rad image analysis system (Bio-Rad Laboratories, Hercules, CA, USA) and analyzed with Quantity One v4.6.2 software. The relative expression of the proteins was expressed by the ratio of gray value of each protein to that of internal reference GAPDH.

Statistical analysis

Statistical analysis was conducted using SPSS 21.0 statistical software (IBM, Armonk, NY, USA). Measurement data were summarized by mean ± standard deviation. When data were in normal distribution and homogeneity, data between two unpaired groups were compared by unpaired t-test. Measurement data among multiple groups were compared by one-way analysis of variance (ANOVA) with Tukey's *post hoc* test. Data comparison among multiple groups at different time points was conducted using repeated measurement ANOVA with Bonferroni's *post hoc* test. Pearson's correlation analysis was used to analyze the relationship between indicators. Measurement data were represented by examples, and verified by a chi-square test. A $p < 0.05$ demonstrated statistical significance.

Results

Downregulation of miR-21 inhibits the immunosuppressive ability of MDSCs in lung cancer

Through the R language differential analysis of GSE63805 in the GEO database, we found 19 differentially expressed miRNAs, among which miR-21 exhibited the most significant expression (Fig. 1A). We decided to explore the role and mechanism of miR-21 in the immunosuppressive ability of MDSCs in lung cancer.

First of all, in order to determine the expression of miR-21 in lung cancer, we drew a box line map by extracting the expression data of miR-21 of dataset GSE63805, which found overexpression of miR-21 in lung cancer samples (Fig. 1B). RT-qPCR analysis showed that, compared with normal tissue, the expression of miR-21 in lung cancer tissues was higher. Compared with the mouse lung epithelial cells-12 (MLE-12), miR-21 expression was upregulated in all of the lung cancer cell lines ($p < 0.05$) (Fig. 1C, D). Statistical analysis of the relationship between miR-21 expression and clinical indicators of lung cancer patients showed that the expression level of miR-21 was closely related to tumor size, tumor node metastasis (TNM) stage, smoking history, and presence of lymph node metastasis (Table 2).

Table 2
The relationship between miR-21 expression and cliniccopathological features of lung cancer patients

Clinicopathological features	Cases (n = 30)	miR-21 expression		P value
		High	Low	
Age (years)				0.7047
> 60	23	12	11	
≤ 60	34	16	18	
Gender				0.1885
Male	29	17	12	
Female	28	11	17	
Tumor size (cm)				0.0030
≥ 3.0	33	22	11	
< 3.0	24	6	18	
TNM stage				0.0277
I-II	21	6	15	
IIIa	36	22	14	
Smoking history				0.0167
Smokers	31	20	11	
Non-mokers	26	8	18	
Lymph node metastasis				0.0074
Positive	24	17	7	
Negative	33	11	22	
Histological tumor type				0.2828
Squamous cell carcinoma	19	11	8	
Adenocarcinoma	21	12	9	
Small cell lung cancer	13	4	9	
Large cell lung cancer	4	1	3	

Expression of miR-21 in mice treated with miR-21 antagomir was lower than in mice treated with antagomir NC ($p < 0.05$) (Fig. 1E). In modeled mice, the proportion of MDSCs with $CD11b^{+}Gr\text{-}1^{+}$ in the peripheral blood was increased. Then, we selected peripheral blood and tumor tissues to further evaluate the effect of miR-21 on the immunosuppression of lung cancer. We used a flow cytometer to analyze the proportion of MDSCs, T helper (Th) and cytotoxic T lymphocyte (CTL) in the peripheral blood and tumor tissues of mice treated with miR-21 antagomir. The results indicated that, compared with the antagomir NC, the proportion of MDSCs was notably decreased, while the proportion of Th and CTL was increased in mice treated with miR-21 antagomir ($p < 0.05$) (Fig. 1F, G). Next, $CD4^{+}$ or $CD8^{+}$ T cells labeled with CFSC were detected by flow cytometry (Fig. 1H), which revealed that, compared with mice treated with antagomir NC, MDSCs in the peripheral blood and tumor tissues of mice injected with miR-21 antagomir markedly reduced the inhibition on the proliferation of Th and CTL ($p < 0.05$) (Fig. 1I, J). Then the expression of MDSCs functional markers ARG-1, iNOS was measured by RT-qPCR and western blot analysis, which showed markedly reduced expression of ARG-1, iNOS in the mice injected with miR-21 antagomir compared with the NC ($p < 0.05$) (Fig. 1K. L). ELISA analysis showed that IL-10, TGF-β and GM-CSF levels in the mice injected with miR-21 antagomir were much lower than the NC (Fig. 1M). Therefore, downregulated miR-21 can retard the immunosuppressive ability of MDSCs on lung cancer.

miR-21 promotes the expression of YAP by inhibiting RUNX1

To further examine the downstream regulatory mechanism of miR-21, we obtained 2290 downstream target genes of miR-21 through mirDIP and 1273 through starBase, and 4036 differentially expressed genes in lung cancer by analysis of the GSE74706 dataset in the GEO database (Fig. 2A). We compared the predicted downstream target gene of miR-21 with the differentially expressed gene and the human transcription factors in Cistrome, and selected 8 transcription factors with significant differences in the downstream target genes of miR-21 in lung cancer (Fig. 2B). GeneMANIA found of 20 genes related to RUNX1 (Fig. 2B), and Cistrome predicted 485 highly correlated target genes of RUNX1 in lung adenocarcinoma. We took the intersection of GeneMANIA and Cistrome results to identify the key downstream target of RUNX1, which proved to be YAP1 (Fig. 2D). Through GEPIA analysis of lung adenocarcinoma and lung squamous cell carcinoma data in the TCGA database, we found that RUNX1 and YAP1 were negatively correlated (Fig. 2E). Besides, the starbase website predicted that miR-21 could inhibit the expression of transcription factor RUNX1 (Fig. 2F). Therefore, we speculated that miR-21 might regulate YAP expression by inhibiting RUNX1 expression in mice.

The microarray-based analysis suggested the presence of binding sites between miR-21 and RUNX1 (Fig. 2F). At the same time, the targeting relationship between miR-21 and RUNX1 was confirmed by the dual luciferase reporter gene assay, which showed that the fluorescence intensity of cells co-transfected with miR-21 inhibitor and RUNX1-WT was higher than that in cells treated with miR-21 NC only ($p < 0.05$), while there was no such significant difference in the cells co-transfected with miR-21 inhibitor and RUNX1-WT ($P > 0.05$) (Fig. 2G). The combination of miR-21 and RUNX1 detected by RIP assay indicated

greater enrichment of miR-21 and RUNX1 in cells treated with Ago2 group than cells treated with IgG ($p < 0.05$) (Fig. 2H).

Immunohistochemistry results showed that, compared with the NC, the expression of RUNX1 in tumor bearing mice was lower, while the expression of YAP was increased ($p < 0.05$) (Fig. 2I). Then, RUNX1 was knocked-down to interfere specifically with the small RNAs, and the interference efficiency was detected. Results showed that, compared with the cells treated with sh-NC, the expression of RUNX1 was notably decreased in cells treated with sh-RUNX1-1, sh-RUNX1-2, and sh-RUNX1-3 ($p < 0.05$), indicating that the low expression vector was successfully transfected. The expression of RUNX1 in cells treated with sh-RUNX1-3 decreased most significantly, so it was selected for the following experiments (Fig. 2J).

The results of RT-qPCR showed that the mRNA expression of YAP in the cells transfected with sh-RUNX1 was higher than in the NC cells ($p < 0.05$) (Fig. 2K). The results of ChIP assay indicated that, compared with the cells treated with IgG, the DNA of YAP gene promoter in cells transfected with RUNX1 was remarkably increased ($p < 0.05$), indicating that the transcription factor RUNX1 regulated YAP expression in the gene promoter region. In addition, when RUNX1 was knocked down in Lewis lung cancer cells, the enrichment of RUNX1 on the YAP gene promoter was reduced ($p < 0.05$) (Fig. 2L). According to the dual luciferase reporter gene assay, the fluorescence intensity of cells co-treated with sh-RUNX1 and YAP-WT was much higher than in the cells treated with sh-NC ($p < 0.05$), while there was no significant difference in the cells co-treated with sh-RUNX1 and YAP-MUT ($p > 0.05$) (Fig. 2M). Then the expression of miR-21 was measured by RT-qPCR (Fig. 2N), while the expression of RUNX1 and YAP (Fig. 2O) was assessed by western blot analysis respectively. These assays showed that the downregulation of YAP mediated by miR-21 antagomir could be reversed by sh-RUNX1 ($p < 0.05$). Finally, Pearson correlation analysis of miR-21 and RUNX1, miR-21 and YAP, RUNX1 and YAP showed that the expression of miR-21 was negatively correlated with that of RUNX1, RUNX1 and YAP, but the expression of miR-21 and YAP was positively correlated. Consequently, miR-21 upregulated YAP through the inhibition of RUNX1.

miR-21 regulates the immunosuppressive ability of MDSCs against lung cancer via promoting the expression of YAP mediated by RUNX1

RT-qPCR showed that the expression of miR-21 in the cells co-treated with miR-21 antagomir and sh-NC, miR-21 antagomir and sh-RUNX1 was lower than in cells with antagomir NC and sh-NC treatments ($p < 0.05$). Furthermore, cells co-treated with miR-21 antagomir and oe-NC, or miR-21 antagomir and oe-YAP exhibited lower miR-21 expression than cells treated with antagomir NC and oe-NC (Fig. 3A). Western blot analysis showed that the level of RUNX1 was notably increased and the level of YAP was lower in the cells co-transfected with miR-21 antagomir and sh-NC compared to cells co-treated with antagomir NC and sh-NC. Compared with the cells co-treated with miR-21 antagomir and sh-NC, the level of RUNX1 was decreased while the level of YAP was dramatically increased in the cells co-transfected with miR-21 antagomir and sh-RUNX1. Compared with the cells co-treated with antagomir NC and oe-NC, the level of

RUNX1 was increased while the level of YAP was notably decreased in the cells co-transfected with miR-21 antagomir and oe-NC. The expression of RUNX1 was much lower while the expression of YAP was much higher in the cells co-transfected with miR-21 antagomir and oe-YAP than that in the cells co-treated with miR-21 antagomir and oe-NC ($p < 0.05$) (Fig. 3B).

Then, flow cytometry was performed to measure the proportion of MDSCs, Th and CTL in the peripheral blood and tumor tissues of the mice, which indicated that the proportion of MDSCs was dropped while the proportion of Th and CTL was dramatically increased in the cells co-transfected with miR-21 antagomir and sh-NC compared to the cells co-treated with antagomir NC and sh-NC, while opposite results were observed in cells co-transfected with miR-21 antagomir and sh-RUNX1 in relation to cells co-treated with miR-21 antagomir and sh-NC. The proportion of MDSCs was remarkably reduced while the proportion of Th and CTL was higher in the cells co-transfected with miR-21 antagomir and oe-NC than that in the cells co-treated with antagomir NC and oe-NC. In contrast to the cells co-treated with miR-21 antagomir and oe-NC, the proportion of MDSCs was highly increased while the proportion of Th and CTL was decreased in the cells co-transfected with miR-21 antagomir and oe-YAP ($p < 0.05$) (Fig. 3C-F).

The MDSCs in the peripheral blood and tumor tissues in the mice treated with both miR-21 antagomir and sh-NC inhibited Th and CTL proliferation compared with that in the mice treated with both antagomir NC and sh-NC, which was relieved by addition of sh-RUNX1. Compared with the mice co-treated with antagomir NC and oe-NC, the MDSCs in peripheral blood and tumor tissues of mice co-treated with miR-21 antagomir and oe-NC inhibited the proliferation of Th and CTL, while it was reciprocal in MDSCs in peripheral blood and tumor tissues of mice injected with miR-21 antagomir and oe-YAP compared with mice treated with both miR-21 antagomir and oe-NC ($p < 0.05$) (Fig. 3G-H).

ELISA assay showed that the expression of IL-10, TGF-β and GM-CSF in cells co-treated with miR-21 antagomir and sh-NC was dramatically lower than that in cells co-transfected with antagomir NC and sh-NC, while opposite results were seen in cells treated with miR-21 antagomir and sh-RUNX1 in comparison to miR-21 antagomir and sh-NC. The levels of IL-10, TGF-β and GM-CSF were decreased in the cells treated with miR-21 antagomir and oe-NC than that in the cells treated with both antagomir NC and oe-NC, but opposite results were witnessed in cells treated with both miR-21 antagomir and oe-YAP than that co-treated with miR-21 antagomir and oe-NC ($p < 0.05$) (Fig. 3I).

Then, the mRNA and protein expression of ARG-1 and iNOS, the two functional markers of MDSCs, was analyzed by RT-qPCR and western blot analysis. The results showed lower expression of mRNA and protein of ARG-1 and iNOS in the cells transfected with both miR-21 antagomir and sh-NC compared to cells co-treated with antagomir NC and sh-NC. However, expression levels were higher in the cells transfected with both miR-21 antagomir and sh-RUNX1 compared with the cells co-treated with miR-21 antagomir and sh-NC. Expression levels were decreased in the cells co-transfected with miR-21 antagomir and oe-NC when compared with the cells treated with both antagomir NC and oe-NC, which was reversed by co-treatment with miR-21 antagomir and oe-YAP (Fig. 3J). Consequently, miR-21 can regulate YAP by regulating the expression of RUNX1 to mediate the immunosuppressive ability of MDSCs in lung cancer.

Immunosuppressive effect of the miR-21/RUNX1/YAP axis in regulating the cell cycle and apoptosis of MDSCs in vitro

We further studied the effects of miR-21/RUNX1/YAP axis on MDSCs cycle, apoptosis and key immunosuppressive molecules *in vitro*. MDSCs purity of the $CD11b^{+}Gr\text{-}1^{+}$ phenotype increased from 21.2–96.6% after magnetic bead separation, indicating that the magnetic bead separation successfully enriched the MDSCs with $CD11b^{+}Gr\text{-}1^{+}$ phenotype, which were then used for the following *in vitro* experiments (Fig. 4A).

Flow cytometry was performed to analyze the ability of the miR-21/RUNX1/YAP axis to regulate the cell cycle and apoptosis of MDSCs. The distribution of MDSCs in different states was assessed by AnnexinV and PI double staining. The results showed that the apoptosis rate of MDSCs co-treated with miR-21 antagomir and sh-NC, miR-21 antagomir and oe-NC was enhanced, accompanied by more cells at the G0/G1 phase, fewer cells at G2/M phase with no difference in cells at S phase in comparison to those in MDSCs co-transfected with antagomir NC and sh-NC, antagomir NC and oe-NC, respectively. On the contrary, compared with MDSCs co-treated with miR-21 antagomir and sh-NC, miR-21 antagomir and oe-NC, the apoptosis rate of MDSCs co-transfected with miR-21 antagomir and sh-RUNX1, miR-21 antagomir and oe-YAP was notably decreased, and there were fewer cells at G0/G1 phase, more cells at G2/M phase with no difference in cells at S phase correspondingly ($p < 0.05$) (Fig. 4B-C).

The results of ELISA indicated that, compared with the cells co-treated with antagomir NC and sh-NC, the expression of IL-10, TGF-β and GM-CSF in the cells co-treated with miR-21 antagomir and sh-NC decreased, compared with the latter, and the expression of IL-10, TGF-β and GM-CSF in the cells co-treated with miR-21 antagomir and sh-RUNX1 was increased ($p < 0.05$). The levels of IL-10, TGF-β and GM-CSF in the cells co-treated with miR-21 antagomir and oe-NC were much lower than in the cells transfected with antagomir NC and oe-NC in combination, while it was opposite in the cells co-treated with miR-21 antagomir and oe-YAP compared to those in the cells co-treated with miR-21 antagomir and oe-NC ($p < 0.05$) (Fig. 4D).

RT-qPCR and western blot analysis suggested that the mRNA and protein expression of ARG-1 and iNOS in the cells treated with both miR-21 antagomir and sh-NC was lower than that in the cells treated with both antagomir NC and sh-NC, but in the cells co-treated with miR-21 antagomir and sh-RUNX1, mRNA and protein expression of ARG-1 and iNOS was notably higher than the former ($p < 0.05$). In comparison to cells transfected with antagomir NC and oe-NC, cells treated with miR-21 antagomir and oe-NC showed lower mRNA and protein expression of ARG-1 and iNOS. Compared with the cells transfected with miR-21 antagomir and oe-NC in combination, mRNA and protein expression of ARG-1 and iNOS in the cells co-treated with antagomir NC and oe-NC, miR-21 antagomir and oe-YAP was higher (Fig. 4E). Collectively, miR-21/RUNX1/YAP axis promoted the cycle and apoptosis of MDSCs and inhibited the key immunosuppressive molecules.

miR-21 promotes tumor development through promoting the expression of YAP mediated by RUNX1 in vivo

The average tumor volume and weight in mice co-treated with miR-21 antagomir and sh-NC were lower than that in mice injected with antagomir NC and sh-NC. However, compared with the mice inoculated with both miR-21 antagomir and sh-NC, the average tumor volume and weight in mice inoculated with both miR-21 antagomir and sh-RUNX1 were increased ($p < 0.05$). Compared with the mice co-treated with antagomir NC and oe-NC, the average tumor volume and weight in mice co-treated with miR-21 antagomir and oe-NC were decreased, compared with the latter, the average tumor volume and weight in mice co-treated with miR-21 antagomir and oe-YAP were increased ($p < 0.05$) (Fig. 5A-C).

The results of RT-qPCR showed that the expression of ARG-1 and iNOS in the mice treated with both miR-21 antagomir and sh-NC was lower than that in the mice treated with both antagomir NC and sh-NC, but that in the mice co-treated with miR-21 antagomir and sh-RUNX1 was notably higher than the former ($p < 0.05$). The levels of ARG-1 and iNOS in the mice co-treated with miR-21 antagomir and oe-NC were much lower than in the mice injected with antagomir NC and oe-NC in combination. However, but the expression of ARG-1 and iNOS in the mice co-treated with miR-21 antagomir and oe-YAP were much higher than in the mice co-treated with miR-21 antagomir and oe-NC ($p < 0.05$) (Fig. 5D).

RT-qPCR results showed that the expression of miR-21 in the mice co-treated with miR-21 antagomir and sh-NC, miR-21 antagomir and sh-RUNX1 was lower than that in the mice co-treated with antagomir NC and sh-NC ($p < 0.05$). Compared with the mice co-treated with antagomir NC and oe-NC, the level of miR-21 in the mice inoculated with both miR-21 antagomir and oe-NC, miR-21 antagomir and oe-YAP was unaffected ($p < 0.05$) (Fig. 5E).

Western blot analysis indicated that the protein level of RUNX1 was notably increased but the protein level of YAP, ARG-1 and iNOS was remarkably decreased in the mice co-treated with miR-21 antagomir and sh-NC compared to that in the mice co-treated with antagomir NC and sh-NC, while it was reciprocal in mice co-treated with miR-21 antagomir and sh-RUNX1 compared with miR-21 antagomir and sh-NC ($p < 0.05$). Compared with the mice co-treated with antagomir NC and oe-NC, the protein level of RUNX1 was increased while the protein levels of YAP, ARG-1 and iNOS were notably decreased in the mice co-transfected with miR-21 antagomir and oe-NC, but the results were opposite in the mice co-treated with miR-21 antagomir and oe-YAP than the latter ($p < 0.05$) (Fig. 5F). In conclusion, miR-21 promotes tumor development through elevating the expression of RUNX1-mediated YAP.

Discussion

As a main cause of cancer-related death among men and women, the occurrence of lung cancer has a close link with smoking and the use of tobacco products, as well as such environmental factors as air pollution [17]. Although chemotherapy and the integration of targeted therapy for lung cancer have made some progress, the overall effect is still not satisfactory with respect to long term survival [18]. At the

same time, the understanding of the molecular mechanisms of tumor immunology, especially the inhibition of anti-tumor immune response mediated by immune synapses or immune checkpoints, has grown rapidly in the past decade [19]. Therefore, the purpose of this study is to explore the specific molecular mechanism of miR-21 on the immunosuppressive ability of MDSCs against lung cancer.

Certain miRNAs can regulate the differentiation, maturation and function of immune cells, and thus act as important contributors in maintaining cellular homeostasis and the development of distinct physiological systems [20]. Initially, our study found that miR-21 was upregulated in the lung cancer, which was in line with findings provided by Wu *et al*. [21]. Similarly, miR-21 was reported to be highly expressed in NSCLC and regulates invasion and chemo-sensitivity of the cancer by mediating SMAD7 [22]. In addition, downregulation of miR-21 inhibits proliferation and migration of non-small cell lung cancer cells by mediating programmed cell death 4 [23]. However, it is not clear whether and how miR-21 participates in the differentiation and functional regulation of MDSCs. ELISA, T cell proliferation analysis and immunohistochemistry suggested that downregulation of miR-21 can inhibit the immunosuppressive ability of MDSCs to lung cancer. Similarly, others have shown that miR-21 can regulate the immune resistance of myelogenous suppressor cells to tumor [24].

On the other hand, RUNX1 was predicted the downstream target gene of miR-21 by mirDIP and starBase. Indeed, RUNX1 is an important regulator of hematopoiesis, and is known to be related to the enhancement of metastasis [25]. Furthermore, miR-9 regulated MDSCs differentiation by targeting RUNX1, an essential transcription factor in regulating MDSC differentiation and function [20]. In our study, RUNX1 was downregulated in the lung cancer. Similarly, RUNX1 is downregulated and negatively correlated with MDSC-mediated immunosuppression in lung cancer [26]. Also, Rasip1 is regulated by the transcription factor RUNX1 to promote migration of NSCLC [25]. According to the intersection of GeneMANIA and Cistrome results, YAP is the downstream target of RUNX1 in lung cancer. Previous research has shown that RUNX1 can inhibit YAP expression to accelerate the occurrence of tumors and inhibit the expression of its target gene [13]. YAP is a highly expressed tumor protein in NSCLC, which plays an important role in regulating the growth and invasion of tumor cells [27]. Furthermore, YAP promotes tumor development through regulating the infiltration of MDSCs [28, 29]. Hence, our study suggested that miR-21 can upregulate the level of YAP by targeting RUNX1 to regulate the immunosuppressive ability of MDSCs in lung cancer.

A previous study has indicated that overexpression of miR-21 increased invasion of MCF-7 cancer cells, and enhanced EGF-mediated invasion and TGF-β-mediated invasion in breast cancer [30]. In addition, miR-21 functions as an upstream regulator of IL-10 by targeting the 3' untranslated region of IL-10 mRNA [31]. Recently, it was demonstrated that miR-21 targets IL-10 mRNA and plays a proinflammatory role by retarding IL-10-expressing regulatory B cell (B10) differentiation [32]. Similarly, the ELISA results in our study indicated that silencing miR-21 can inhibit the expression of IL-10, TGF-β and GM-CSF, which was reserved by silencing RUNX1. All in all, miR-21/RUNX1/YAP axis can promote the cycle and apoptosis of MDSCs, and inhibit the effect of key immunosuppressive molecules.

Taken together, the upregulation of miR-21 inhibits the expression of the downstream target gene RUNX1 in lung cancer. RUNX1 can bind to the promoter region of YAP to downregulate its expression. We conclude that miR-21 upregulated YAP expression by inhibiting the transcription factor RUNX1 to regulate the immunosuppressive ability of MDSCs against lung cancer (Fig. 6). Our findings not only improved the understanding of how miR-21 modulates the immunosuppressive ability of MDSCs in lung cancer, but also offered a potential prognostic marker and a therapeutic target for lung cancer.

Abbreviations

miR-21: microRNA-21; MDSCs: myeloid-derived suppressor cells; Th: T helper; GEO: Gene Expression Omnibus; TCGA: the Cancer Genome Atlas; GEPIA: Gene Expression Profiling Interactive Analysis; DMEM: Dulbecco's Modified Eagle Medium; PBS: phosphate buffer saline; NC: negative control; CFSE: carboxyfluorescein diacetate, succinimidylester; PI: propidium iodide; RIPA: radio-immunoprecipitation assay; GAPDH: glyceraldehyde-3-phosphate dehydrogenase; PMSF: phenylmethylsulfonyl fluoride; BCA: Bicinchoninic acid; SDS: sodium dodecyl sulfate; SDS-PAGE: sodium dodecyl sulfate–polyacrylamide electrophoresis; PVDF: polyvinylidene fluoride.

Declarations

Acknowledgements

We would like to acknowledge the colleagues for their helpful assistance on this study.

Author contributions

Guangping Meng and Jie Zhang conceived and designed research. Danhua Qu and Yanjun Wang performed experiments. Jinying Wei analyzed data. Danhua Qu interpreted results of experiments. Jinying Wei prepared figures. Guangping Meng and Jie Zhang drafted manuscript. Yanjun Wang edited and revised manuscript. Guangping Meng, Jinying Wei, Yanjun Wang, Danhua Qu and Jie Zhang approved final version of manuscript.

Funding

This study was supported by General Programs of National Natural Science Foundation of China (No. 81672297).

Availability of data and materials

The authors confirm that the data supporting the findings of this study are available within the article

Ethics approval and consent to participate

All animal experiments and procedures were approved by the Institutional Animal Care and Use Committee of the Second Hospital of Jilin University. The animal experiments were conducted based on minimized animal numbers and discomfort of experimental animals.

Consent For Publication

Not applicable.

Competing interests

The authors declare no conflicts of interest.

References

1. Bray F, Ferlay J, Soerjomataram I, Siegel RL, Torre LA, Jemal A. Global cancer statistics 2018: GLOBOCAN estimates of incidence and mortality worldwide for 36 cancers in 185 countries. CA Cancer J Clin. 2018;68:394–424.
2. Cheung CHY, Juan HF. Quantitative proteomics in lung cancer. J Biomed Sci. 2017;24:37.
3. Yousefı M, Bahrami T, Salmaninejad A, Nosrati R, Ghaffari P, Ghaffari SH. Lung cancer-associated brain metastasis: Molecular mechanisms and therapeutic options. Cell Oncol (Dordr). 2017;40:419–41.
4. Duruisseaux M, Esteller M. Lung cancer epigenetics: From knowledge to applications. Semin Cancer Biol. 2018;51:116–28.
5. Wang DC, Wang X. Tomorrow's genome medicine in lung cancer. Semin Cancer Biol. 2017;42:39–43.
6. Liu B, Sun G. Transcriptome and miRNAs analyses enhance our understanding of the evolutionary advantages of polyploidy. Crit Rev Biotechnol. 2019;39:173–80.
7. Leonetti A, Assaraf YG, Veltsista PD, El Hassouni B, Tiseo M, Giovannetti E. MicroRNAs as a drug resistance mechanism to targeted therapies in EGFR-mutated NSCLC: Current implications and future directions. Drug Resist Updat. 2019;42:1–11.
8. Ren W, Hou J, Yang C, Wang H, Wu S, Wu Y, et al. Extracellular vesicles secreted by hypoxia pre-challenged mesenchymal stem cells promote non-small cell lung cancer cell growth and mobility as well as macrophage M2 polarization via miR-21-5p delivery. J Exp Clin Cancer Res. 2019;38:62.

9. Zhou B, Wang D, Sun G, Mei F, Cui Y, Xu H. Effect of miR-21 on Apoptosis in Lung Cancer Cell Through Inhibiting the PI3K/ Akt/NF-kappaB Signaling Pathway in Vitro and in Vivo. Cell Physiol Biochem. 2018;46:999–1008.
10. de Bruijn M, Dzierzak E. Runx transcription factors in the development and function of the definitive hematopoietic system. Blood. 2017;129:2061–9.
11. Maeda R, Sato S, Obata S, Ohno T, Hashiya K, Bando T, et al. Molecular Characteristics of DNA-Alkylating PI Polyamides Targeting RUNX Transcription Factors. J Am Chem Soc. 2019;141:4257–63.
12. Sood R, Kamikubo Y, Liu P. Role of RUNX1 in hematological malignancies. Blood. 2017;129(15):2070–2082. Blood. 2018;131:373.
13. Kulkarni M, Tan TZ, Syed Sulaiman NB, Lamar JM, Bansal P, Cui J, et al. RUNX1 and RUNX3 protect against YAP-mediated EMT, stem-ness and shorter survival outcomes in breast cancer. Oncotarget. 2018;9:14175–92.
14. Kim MH, Kim CG, Kim SK, Shin SJ, Choe EA, Park SH, et al. YAP-Induced PD-L1 Expression Drives Immune Evasion in BRAFi-Resistant Melanoma. Cancer Immunol Res. 2018;6:255–66.
15. Moya IM, Halder G. Hippo-YAP/TAZ signalling in organ regeneration and regenerative medicine. Nat Rev Mol Cell Biol. 2019;20:211–26.
16. Zhao H, Wang X, Yi P, Si Y, Tan P, He J, et al. KSRP specifies monocytic and granulocytic differentiation through regulating miR-129 biogenesis and RUNX1 expression. Nat Commun. 2017;8:1428.
17. Lemjabbar-Alaoui H, Hassan OU, Yang YW, Buchanan P. Lung cancer: Biology and treatment options. Biochim Biophys Acta. 2015;1856:189–210.
18. Byron E, Pinder-Schenck M. Systemic and targeted therapies for early-stage lung cancer. Cancer Control. 2014;21:21–31.
19. Kumar R, Collins D, Dolly S, McDonald F, O'Brien MER, Yap TA. Targeting the PD-1/PD-L1 axis in non-small cell lung cancer. Curr Probl Cancer. 2017;41:111–24.
20. Tian J, Rui K, Tang X, Ma J, Wang Y, Tian X, et al. MicroRNA-9 Regulates the Differentiation and Function of Myeloid-Derived Suppressor Cells via Targeting Runx1. J Immunol. 2015;195:1301–11.
21. Wu D, Shi M, Fan XD. Mechanism of miR-21 via Wnt/beta-catenin signaling pathway in human A549 lung cancer cells and Lewis lung carcinoma in mice. Asian Pac J Trop Med. 2015;8:479–84.
22. Lin L, Tu HB, Wu L, Liu M, Jiang GN. MicroRNA-21 Regulates Non-Small Cell Lung Cancer Cell Invasion and Chemo-Sensitivity through SMAD7. Cell Physiol Biochem. 2016;38:2152–62.
23. Yang Y, Meng H, Peng Q, Yang X, Gan R, Zhao L, et al. Downregulation of microRNA-21 expression restrains non-small cell lung cancer cell proliferation and migration through upregulation of programmed cell death 4. Cancer Gene Ther. 2015;22:23–9.
24. Li L, Zhang J, Diao W, Wang D, Wei Y, Zhang CY, et al. MicroRNA-155 and MicroRNA-21 promote the expansion of functional myeloid-derived suppressor cells. J Immunol. 2014;192:1034–43.

25. Chen Y, Zhang L, Liu L, Sun S, Zhao X, Wang Y, et al. Rasip1 is a RUNX1 target gene and promotes migration of NSCLC cells. Cancer Manag Res. 2018;10:4537–52.
26. Tian X, Ma J, Wang T, Tian J, Zheng Y, Peng R, et al. Long non-coding RNA RUNXOR accelerates MDSC-mediated immunosuppression in lung cancer. BMC Cancer. 2018;18:660.
27. Wang Y, Dong Q, Zhang Q, Li Z, Wang E, Qiu X. Overexpression of yes-associated protein contributes to progression and poor prognosis of non-small-cell lung cancer. Cancer Sci. 2010;101:1279–85.
28. Wang G, Lu X, Dey P, Deng P, Wu CC, Jiang S, et al. Targeting YAP-Dependent MDSC Infiltration Impairs Tumor Progression. Cancer Discov. 2016;6:80–95.
29. Zhang S, Liu Z, Wu L, Wang Y. MiR-361 targets Yes-associated protein (YAP) mRNA to suppress cell proliferation in lung cancer. Biochem Biophys Res Commun. 2017;492:468–73.
30. Han M, Wang F, Gu Y, Pei X, Guo G, Yu C, et al. MicroRNA-21 induces breast cancer cell invasion and migration by suppressing smad7 via EGF and TGF-beta pathways. Oncol Rep. 2016;35:73–80.
31. Wang H, Xu W, Shao Q, Ding Q. miR-21 silencing ameliorates experimental autoimmune encephalomyelitis by promoting the differentiation of IL-10-producing B cells. Oncotarget. 2017;8:94069–79.
32. Wang H, Fan H, Tao J, Shao Q, Ding Q. MicroRNA-21 silencing prolongs islet allograft survival by inhibiting Th17 cells. Int Immunopharmacol. 2019;66:274–81.

Figures

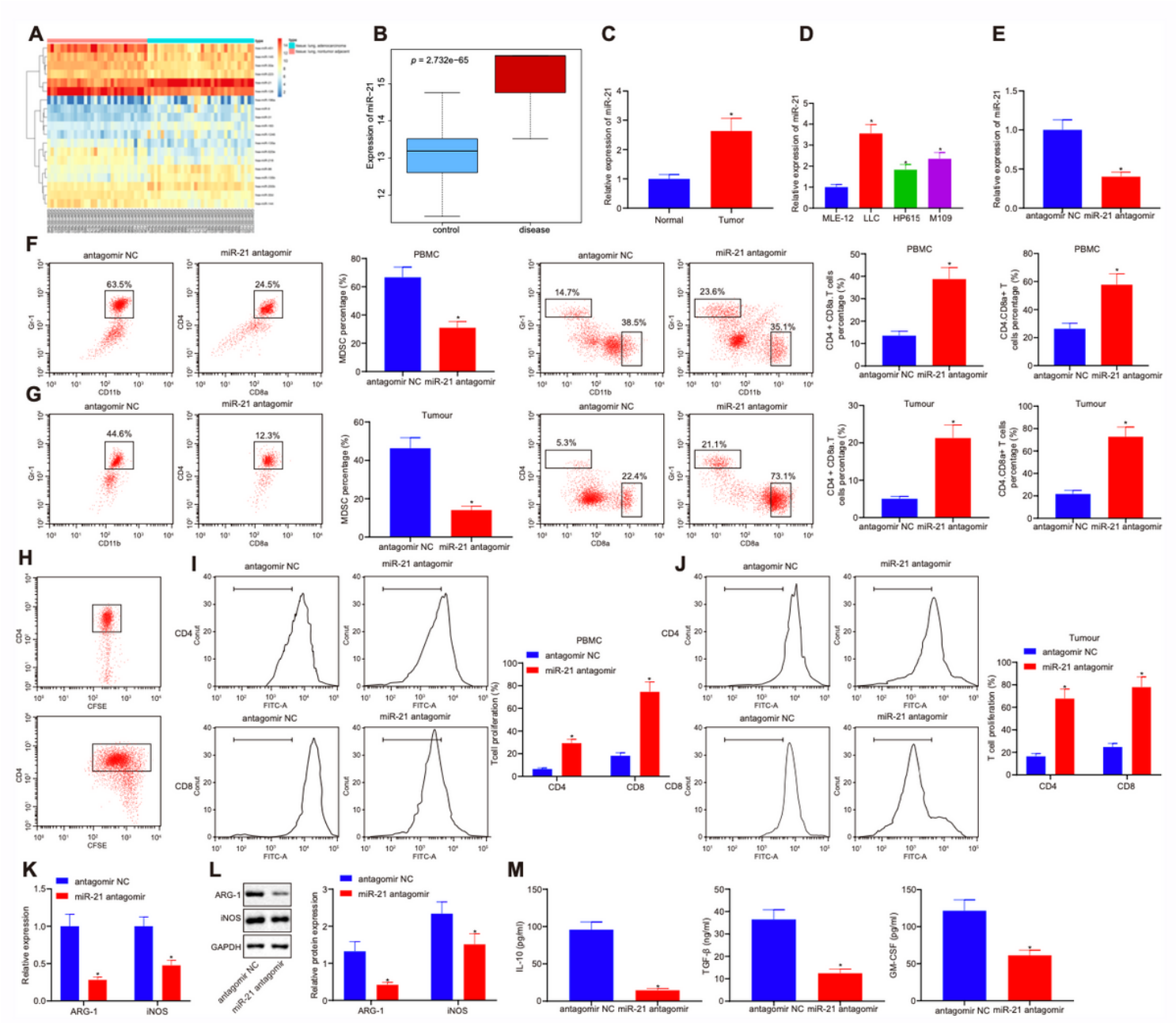

Figure 1

Downregulation of miR-21 inhibits the immunosuppressive ability of MDSCs in lung cancer. A, heat map of 19 different miRNAs of dataset GSE63805; B, box line map of miR-21 of dataset GSE63805, the blue box on the left shows the expression of normal samples, and the red box on the right shows the expression of lung cancer samples (P = 2.732e - 65); C, D, miR-21 expression in lung cancer cells analyzed by RT-qPCR (n = 57), * p < 0.05 vs. the normal cells; # p < 0.05 vs. the MLE-12; E, the relative expression of miR-21 measured by RT-qPCR; F, G, the proportion of MDSCs, Th, CTL in the peripheral blood and tumor tissues of mice measured by a flow cytometer; H, CD4+ or CD8+ T cells labeled with CFSC detected by flow cytometry; I, J, the inhibition effect of MDSCs on Th, CTL detected by T cell proliferation analysis; K, the expression of ARG-1 and iNOS measured by RT-qPCR; L, the expression of ARG-1 and iNOS protein measured by western blot analysis; M, the expression of IL-10, TGF-β and GM-

CSF analyzed by ELISA. * p < 0.05 vs. antagomir NC. The data in the Fig.s were all measurements, expressed as mean ± standard deviation; n=12. Data between two unpaired groups were compared by unpaired t-test. One-way ANOVA with Tukey's post hoc test was used to compare data among multiple groups. The experiment was repeated three times.

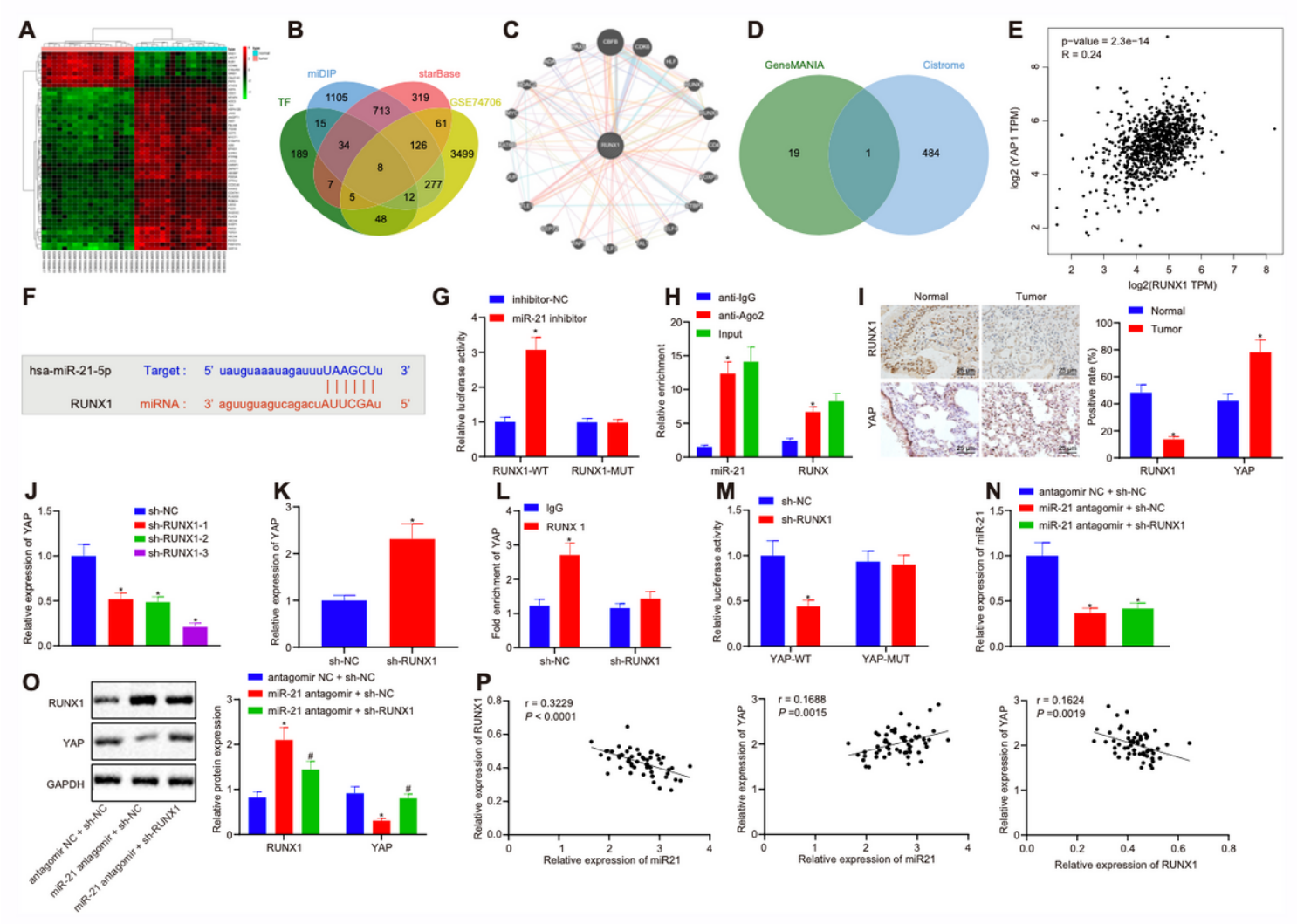

Figure 2

miR-21 upregulates YAP expression via inhibiting RUNX1. A, heat map of 50 genes of dataset GSE74706; B, downstream genes of miR-21 and significant differentially expressed genes of dataset GSE74706 predicted by mirDIP and starBase and the Venn map of human transcription factor obtained from Cistrome, with BCL11A, E2F3, ERG, ETS1, KLF5, MEF2A, RUNX1 and TTF2 as the intersection genes; C, PPI map of RUNX1 and its related genes obtained from GeneMANIA; D, Venn map of genes related to RUNX1 obtained from GeneMANIA and target genes of RUNX1 predicted by Cistrome in lung adenocarcinoma, with YAP1 (YAP) as the only intersection gene; E, correlation of RUNX1 and YAP1 in lung adenocarcinoma and squamous cell carcinoma of TCGA database analyzed by GEPIA (P = 2.3e-14); F, binding site sequences of miR-21 and RUNX1; G, relationship between miR-21 and RUNX1 measured by dual luciferase reporter gene assay, * p < 0.05 vs. miR-21; H, binding of miR-21 and RUNX1 analyzed by RIP, * p < 0.05 vs. anti-IgG1; I, the expression of RUNX1 and YAP in tumor tissues measured by

immunohistochemistry, * $p < 0.05$ vs. normal mice; J, the expression of RUNX1 after transfection in tissues; K, the expression of YAP when RUNX1 was silenced; L, the binding of RUNX1 and YAP detected by ChIP assay, * $p < 0.05$ vs. IgG; M, the binding of RUNX1 and YAP verified by dual luciferase reporter gene assay; N, the expression of miR-21 in cells measured by RT-qPCR; O, the expression of RUNX1 and YAP in cells measured by western blot analysis; P, the correlation of miR-21 and RUNX1, miR-21 and YAP, RUNX1 and YAP analyzed by Pearson. Measurement data were expressed as mean ± standard deviation. When data were homogeneous and of normal distribution, data between two unpaired groups were compared by unpaired t-test. Measurement data among multiple groups were checked by ANOVA with Tukey's post hoc test. Pearson’s correlation analysis was used to analyze the relationships between miR-21, RUNX1 and YAP.

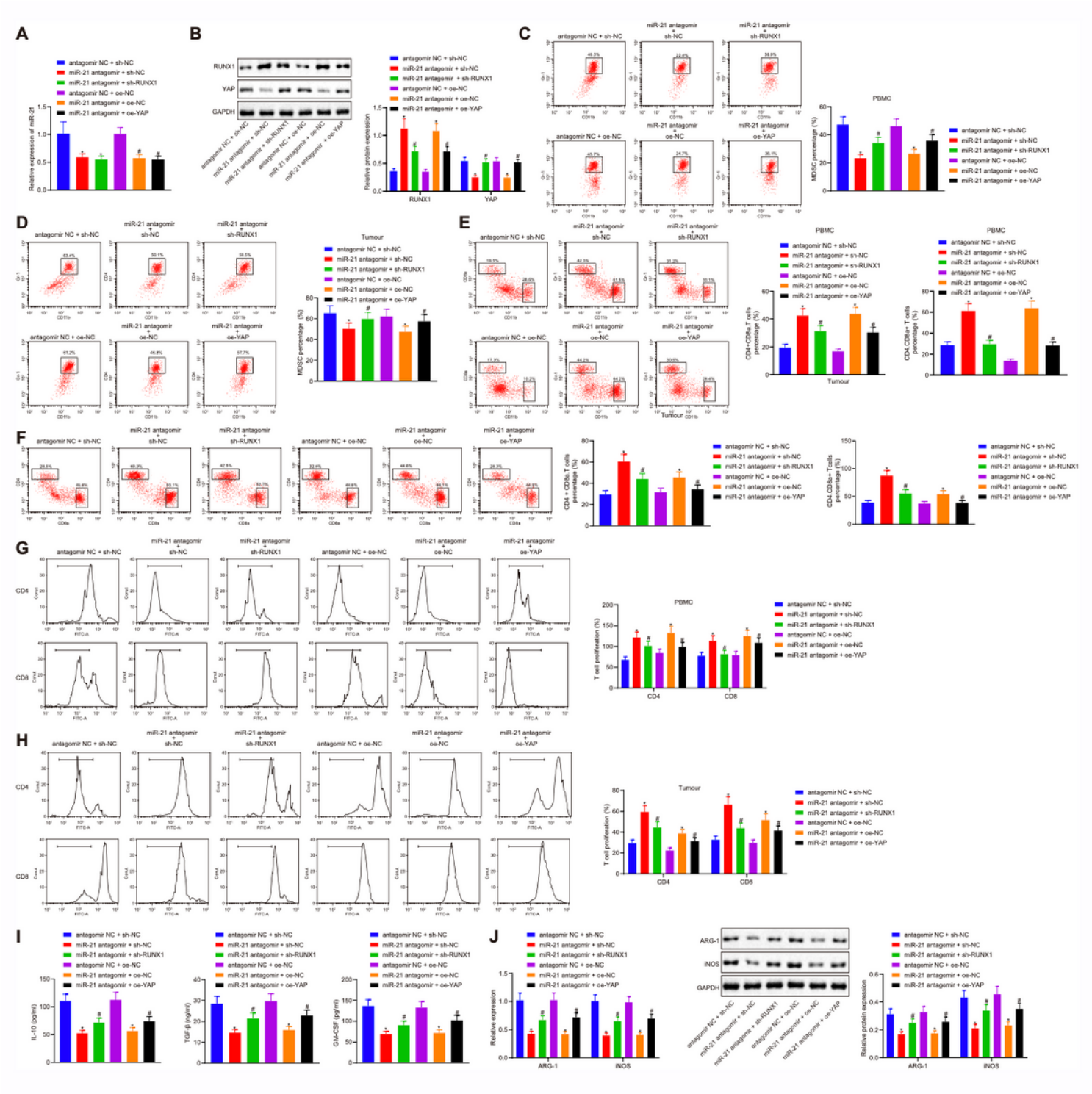

Figure 3

The miR-21/RUNX1/YAP axis regulated the immunosuppressive ability of MDSCs in lung cancer. A, the expression of miR-21 analyzed by RT-qPCR; B, the expression of RUNX1 and YAP measured by western blot analysis; C, D, the proportion of MDSCs in peripheral blood and tumor tissues of mice detected by flow cytometry; E, F, the proportion of Th and CTL in peripheral blood and tumor tissues measured by flow cytometry; G-H, the inhibitory effect of MDSCs on Th and CTL in peripheral blood and tumor tissues of mice analyzed by T cell proliferation assay; I, the expression of IL-10, TGF-β and GM-CSF were detected

by ELISA; J, the expression of ARG-1 and iNOS measured by RT-qPCR and western blot analysis. Measurement data were expressed as mean ± standard deviation. * $p < 0.05$ vs. cells co-treated with antagomir NC and sh-NC or antagomir NC and oe-NC, # $p < 0.05$ vs. cells co-treated with miR-21 antagomir and sh-NC or miR-21 antagomir and oe-NC. Measurement data among multiple groups were compared by one-way ANOVA with Tukey's post hoc test. The experiment was repeated three times.

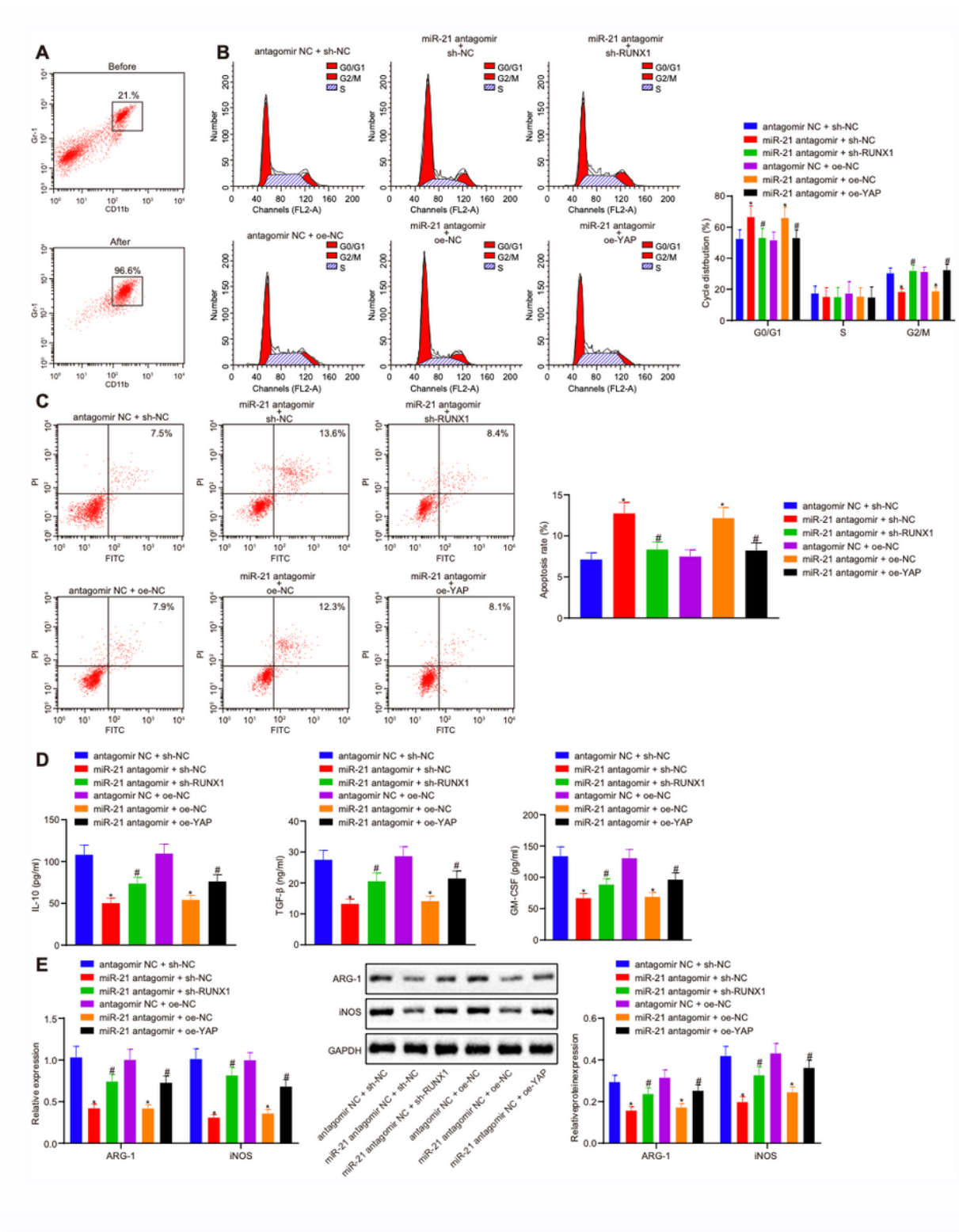

Figure 4

The effect of miR-21/RUNX1/YAP axis on immunosuppressive ability of MDSCs in lung cancer in vitro. A, the proportion of MDSCs in peripheral blood cells before and after magnetic bead sorting; B, the cell cycle of MDSCs analyzed by a flow cytometer; C, apoptosis map of MDSCs after 24 hours treatment; D, the expression of IL-6 and other effectors in MDSCs measured by ELISA; E, the expression of ARG-1 and iNOS detected by RT-qPCR and western blot analysis. Measurement data were expressed as mean ± standard deviation. * $p < 0.05$ vs. cells co-treated with antagomir NC and sh-NC or antagomir NC and oe-NC, # $p < 0.05$ vs. cells co-treated with miR-21 antagomir and sh-NC or miR-21 antagomir and oe-NC. Measurement data among multiple groups were compared by ANOVA with Tukey's post hoc test. The experiment was repeated three times.

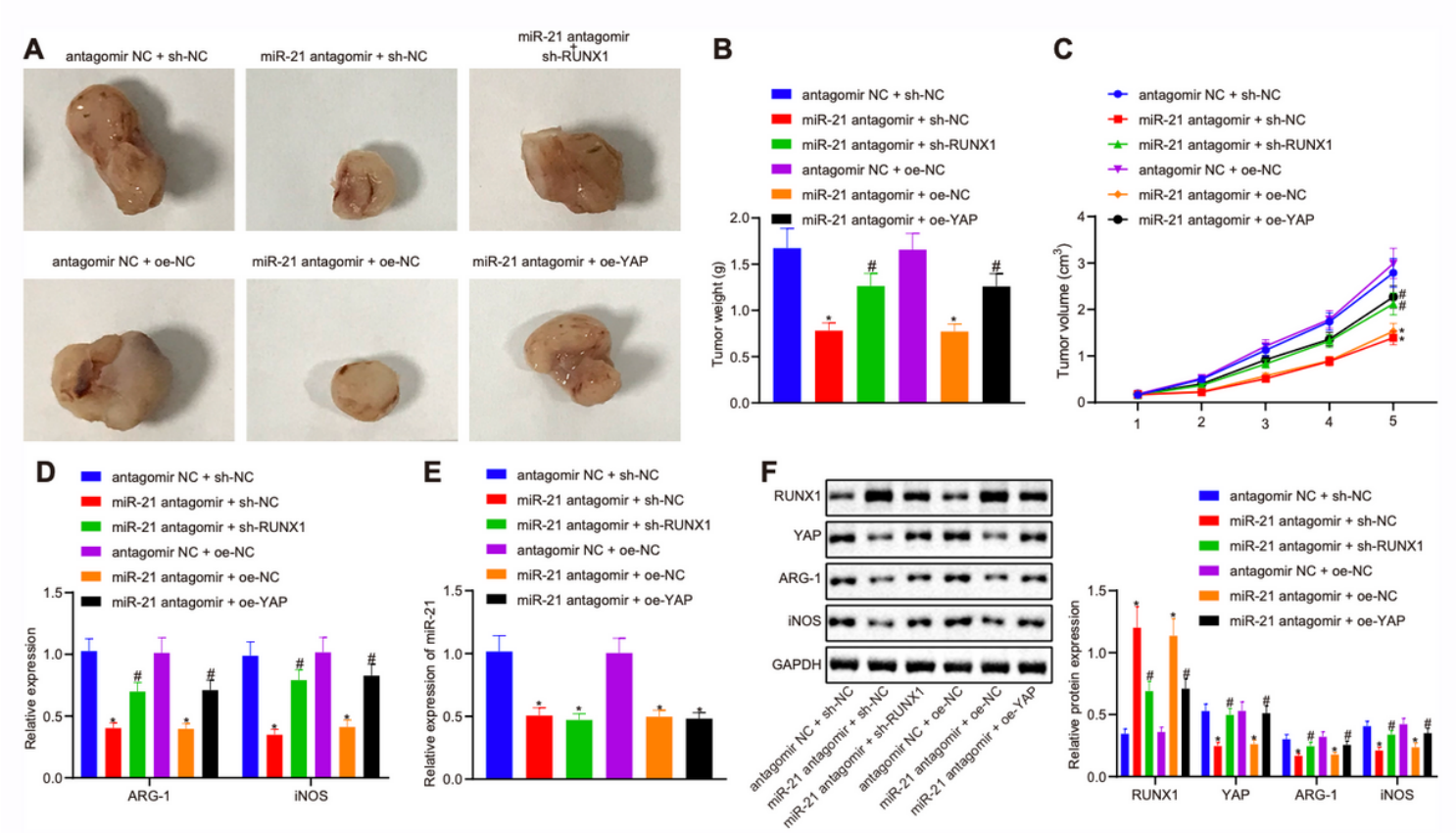

Figure 5

The effect of miR-21/RUNX1/YAP axis on the immunosuppressive ability of lung cancer xenografted tumor in vivo. A, representative image of xenotransplantation tumor formation in nude mice; B, tumor volume of mice; C, tumor mass of mice; D, the expression of ARG-1 and iNOS analyzed by RT-qPCR; E, the expression of miR-21 detected by RT-qPCR; F, the expression of RUNX1, YAP, ARG-1 and iNOS measured by western blot analysis. Measurement data were expressed as mean ± standard deviation. * $p < 0.05$ vs. cells co-treated with antagomir NC and sh-NC or antagomir NC and oe-NC, # $p < 0.05$ vs. cells co-treated with miR-21 antagomir and sh-NC or miR-21 antagomir and oe-NC. Measurement data among multiple groups were checked by ANOVA with Tukey's post hoc test. Data comparison among multiple groups at different time points was conducted using repeated measurement ANOVA with Bonferroni's post hoc test. The experiment was repeated three times.

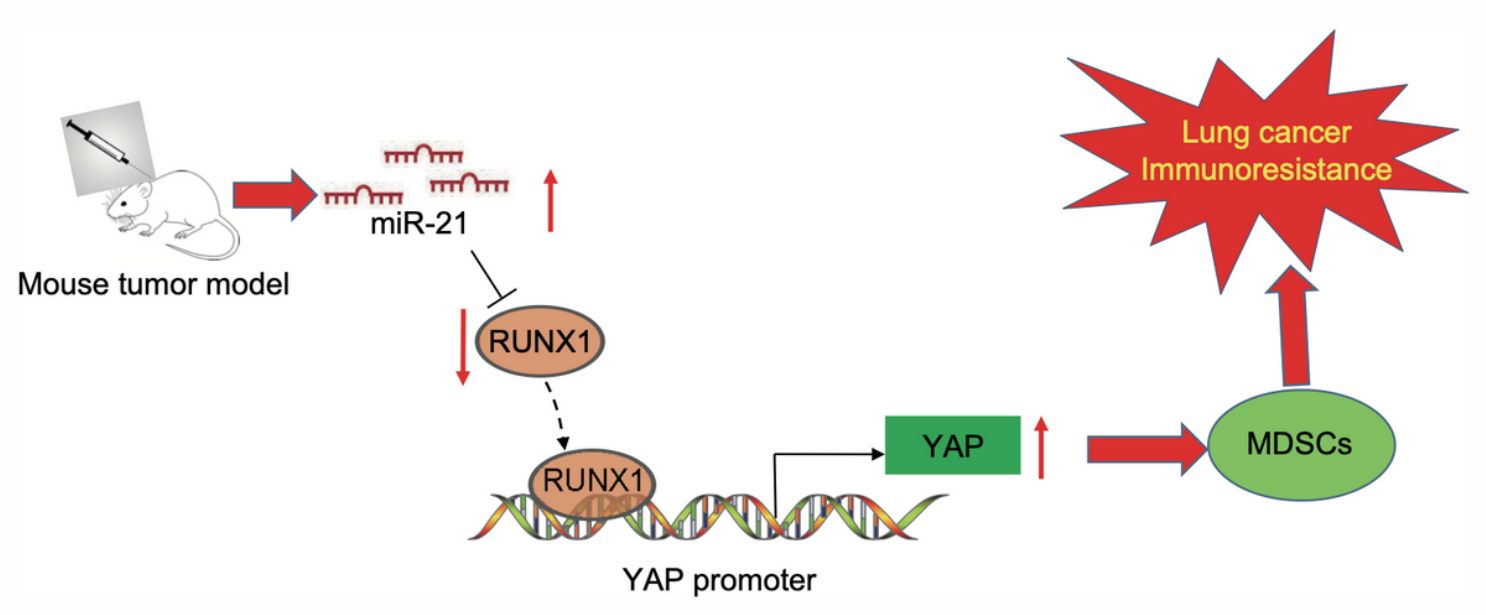

Figure 6

Schematic representation of the potential molecular mechanisms involved in miR-21 in immunosuppressive ability of MDSCs in lung cancer. In lung cancer, upregulated miR-21 inhibits the expression of downstream target gene RUNX1. Since the expression of YAP was mediated through binding with RUNX1 in the promoter region, so the downregulation of RUNX1 can upregulate the expression of YAP, thus inhibiting the immune resistance of MDSCs and promoting the development of tumors.